Local, Three-Dimensional Strain Measurements Within Largely Deformed Extracellular Matrix Constructs

Blayne A. Roeder

Klod Kokini

Department of Biomedical Engineering,
Purdue University, 500 Central Drive,
West Lafayette, IN 47907-2022
and School of Mechanical Engineering,
Purdue University, 585 Purdue Mall,
West Lafayette, IN 47907-2088

J. Paul Robinson

Sherry L. Voytik-Harbin
e-mail: harbins@purdue.edu

Department of Biomedical Engineering,
Purdue University, 500 Central Drive,
West Lafayette, IN 47907-2022, USA and
Department of Basic Medical Sciences,
Purdue University, 625 Harrison Street,
West Lafayette, IN 47907-2026

The ability to create extracellular matrix (ECM) constructs that are mechanically and biochemically similar to those found in vivo and to understand how their properties affect cellular responses will drive the next generation of tissue engineering strategies. To date, many mechanisms by which cells biochemically communicate with the ECM are known. However, the mechanisms by which mechanical information is transmitted between cells and their ECM remain to be elucidated. "Self-assembled" collagen matrices provide an in vitro-model system to study the mechanical behavior of ECM. To begin to understand how the ECM and the cells interact mechanically, the three-dimensional (3D) mechanical properties of the ECM must be quantified at the micro-(local) level in addition to information measured at the macro-(global) level. Here we describe an incremental digital volume correlation (IDVC) algorithm to quantify large ($>$0.05) 3D mechanical strains in the microstructure of 3D collagen matrices in response to applied mechanical loads. Strain measurements from the IDVC algorithm rely on 3D confocal images acquired from collagen matrices under applied mechanical loads. The accuracy and the precision of the IDVC algorithm was verified by comparing both image volumes collected in succession when no deformation was applied to the ECM (zero strain) and image volumes to which simulated deformations were applied in both 1D and 3D (simulated strains). Results indicate that the IDVC algorithm can accurately and precisely determine the 3D strain state inside largely deformed collagen ECMs. Finally, the usefulness of the algorithm was demonstrated by measuring the microlevel 3D strain response of a collagen ECM loaded in tension. [DOI: 10.1115/1.1824127]

Keywords: Extracellular Matrix, Large-Strain, Three-Dimensional, Collagen Fibrils, Biomechanics, Digital Volume Correlation, Digital Image Processing

Introduction

In vivo, the cellular and extracellular matrix (ECM) components of tissues create a dynamic mechanical environment in which loads are communicated in a reciprocal fashion. Such mechanical loads have been identified as critical determinants of fundamental cellular behavior (e.g., adhesion, migration, proliferation, and differentiation) not only during physiological processes but also during the pathogenesis of disease states. In the majority of cases, connective tissue cell types (e.g., smooth muscle cells, fibroblasts, and chondrocytes) experience and exert mechanical loads within the context of a surrounding three-dimensional (3D) ECM. In fact, depending upon the microstructural organization, and mechanical properties of the ECM, as well as the way a cell is attached to its ECM, the deformation applied globally to the tissue may deviate substantially from that actually experienced locally by a cell [1,2]. Unfortunately, the fundamental principles and detailed mechanisms underlying how ECM microstructural and mechanical properties influence the way mechanical loads are transferred between cells and their surrounding ECM (e.g., mechanotransduction) have not been defined, especially within a 3D tissue-like context.

To determine the mechanisms involved in this mechanotransduction process and define their importance in regulating the overall cellular response, a number of experimental approaches and apparatus have been developed (see [1] and [3] for reviews). To study the forces exerted by adherent cells against their supporting substrate or matrix, investigators have plated cells along the surface of flexible substrates fashioned from silicone, polyacrylamide, or collagen and subsequently monitored substrate deformation in 2D [4–6]. An approach that has received widespread use for investigating cell/tissue mechanics within a more 3D physiological context involves the global application of mechanical loads to explanted tissues or 3D tissue constructs formed in vitro. Formation of tissue constructs in vitro routinely consists of seeding cells on or within a 3D scaffold (matrix). For both tissue explants and engineered tissue constructs, the extracellular scaffold and resident cells combine to create a tissue with complex, nonlinear mechanical behavior [7]. Such an approach has shown that mechanical cues affect a number of cellular attributes and that they do so in a cell type-dependent manner. Specifically, mechanical loading of fibroblasts within a type I collagen matrix has been shown to regulate morphology [8], proliferation [9], apoptosis [10], cyclic adenosine monophosphate (CAMP) signaling [11], and expression of gene products, including collagen, matrix proteases, transforming growth factor β, and tenascin C [10,12–16]. However, many of these and other mechanical stimulation studies are nonquantitative with respect to their description of the applied mechanical load. In addition, quantitative information regarding specific structural and mechanical properties of the scaffold at a microscopic level (local to a cell) or a description of how loads are transferred from a macroscopic (global) level to a microscopic (local) level is lacking. Such information is imperative since the magnitude of the load applied to the tissue construct is likely different from that experienced by the cell [1] and the differential load distribution is highly dependent upon the material properties of the scaffold [17].

In many cases, such mechanical loading systems have been adapted with microscopes so that the mechanical loads and their

effects could be better defined at the cellular and subcellular levels. With the advent of confocal laser-scanning microscopy in the mid-1980s and multiphoton imaging technology more recently, 3D spatial information can now be collected from "live," relatively thick specimens, such as tissue explants and engineered tissue constructs, by means of optical sectioning. For example, confocal microscopy has been used previously in a strictly fluorescence mode to monitor changes in cellular and nuclear morphology during compressive loading of articular cartilage explants and chondrocytes grown in 3D scaffolds [18–21]. These studies did not, however, include qualitative or quantitative descriptions of the structural-mechanical properties of the ECM portion of the tissue explants or model tissues.

Recently we have applied confocal microscopy in a reflection (or backscattered light) mode to collect 3D structural information on component fibrils of a collagen ECM as well as resident cells within live specimens [22–24]. Visualization of collagen fibrils, the major structural and mechanical component of ECMs, in their native (unprocessed) state provides for a more accurate description of the cellular microenvironment and facilitates investigation of cell-ECM interactions on an individual cell basis and at a local level. Although cells and their surrounding ECM can be visualized simultaneously using confocal microscopy in a reflection mode, vital fluorochromes that label specific cellular attributes (e.g., membranes) may also be introduced to facilitate discrimination of cell boundaries or to monitor some relevant physiologic process. Other 3D imaging techniques (i.e., magnetic resonance imaging, computer tomography [CT], and microCT) lack the resolution necessary to collect images of individual collagen fibrils comprising the ECM, and of organelles within cells. Of these techniques, microCT has the highest resolving power, but resolution is still limited to approximately 50 μm. Confocal reflection microscopy can resolve features on the order of 0.2 μm.

Most recently, we have integrated a confocal microscope with a miniature mechanical loading instrument to visualize cell-matrix interactions within 3D tissue constructs during mechanical loading. Because this technique does not require fixation or physical sectioning, the response of cells and their associated ECM to various mechanical loads can be monitored in situ over time [25]. While application of confocal microscopy in a reflection or combined reflection-epifluorescence modality can provide new insight into the structural-mechanical properties of the ECM at a microscopic level as well as the mechanisms involved in mechanotransduction, the resultant images contain no inherent quantitative information. To derive relevant micro-mechanical information, including the local strain state of the ECM microstructure, a 3D incremental digital volume correlation (IDVC) technique was developed. Digital volume correlation provides a means by which 3D images of loaded and unloaded structures can be interrogated to determine local displacements and strains. Digital volume correlation is an extension of digital image correlation [26,27], a 2D technique that has found applications in applied mechanics such as high temperature deformation measurements [28] and estimation of stress intensity factors [29]. In fact, 2D image correlation procedures have proven useful for quantification and spatial localization of traction forces exerted by cells as they adhere and migrate along the surface of a deformable substrate [6,30–33]. With respect to tissue mechanics, 2D image correlation procedures have been used to determine the strain distribution within articular cartilage explants during compressive loading [34]. The extension of such correlation procedures to 3D image volumes was originally presented by Bay and coworkers for 3D strain mapping in trabecular bone under compression [35]. Specifically, they used least-squares pattern matching to determine strains based on a pair of 3D microCT images of trabecular bone collected for a single loading step (unloaded and under compression). Their 3D image correlation algorithm was used to determine load induced strains at a tissue level of function or a size scale of ≈ 800–1000 μm. In the present paper, higher resolution 3D imaging techniques involving confocal microscopy in a reflection or combination reflection-epifluorescence mode [22,23,25] were combined with correlation procedures to compute strains on a microscopic or cellular level of function. The IDVC algorithm handles the increased noise characteristics of the confocal images by using cross-correlation pattern matching [36]. Most importantly, application of the IDVC algorithm to confocal image data results in strain measurements on a cellular level of function or a size scale of ≈ 10–20 μm. Last, the IDVC algorithm has the capability to measure strains from a series of 3D images representing incremental changes within the tissue construct as they occur over time or in response to mechanical loading. In this way, the local, 3D micromechanical behavior of tissue explants or constructs can be analyzed in response to both small and large deformations.

The present paper provides a detailed description of this IDVC algorithm as well as an assessment of the algorithm's measurement accuracy and precision. In addition, we report, the application of this algorithm in conjunction with confocal reflection images of mechanically loaded collagen ECM constructs for determination of the 3D strain distribution at a microscopic or local level.

Materials and Methods

Preparation of 3D Collagen ECMs. Native type I collagen prepared from calf skin by acid solubilization was obtained from Sigma Chemical Co. (St. Louis, MO) and dissolved in 0.01 M hydrochloric acid to achieve desired concentrations. Three-dimensional collagen matrices were prepared by neutralizing collagen solutions with 10X phosphate-buffered saline (ionic strength 0.14 M and pH 7.4). Polymerization of neutralized collagen solutions was conducted in a dog bone-shaped mold as described previously [24]. In brief, the mold consisted of a glass plate and a piece of flexible silicone gasket. The gauge section of the mold measured 10 mm long, 4 mm wide, and approximately 1.8 mm thick. Neutralized collagen solution was added to each mold and the mold was incubated at 37°C in a humidified environment. Polypropylene mesh was embedded in the ends of each collagen matrix to facilitate clamping for mechanical loading.

Confocal Imaging During Mechanical Loading. The microstructural deformation experienced by the component fibrils of a 3D collagen ECM during uniaxial tensile loading was monitored in 4D (x, y, z, and time) using an integrated mechanical loading-confocal microscopy setup as described previously [25]. In brief, the mechanical loading-confocal microscopy setup involved interfacing a highly modified Minimat 2000 miniature materials tester (Rheometric Scientific, Inc., Piscataway, NJ) with an MRC 1024 laser scanning confocal microscope (BioRad, Hercules, CA) mounted on a Diaphot 300 microscope (Nikon Corp., Tokyo, Japan). A specially designed adapter plate provided the physical connection between the Minimat and the confocal microscope. This plate possessed a rectangular hole below which a coverglass was bonded, creating a well that allowed the samples to be tested in an aqueous environment representing physiologic temperature, pH, and composition. Optimal positioning of the specimen for confocal imaging was accomplished using clamps that offset the loading axis and maintained the specimen parallel with and close to the coverglass.

Imaging of the collagen ECMs during loading was performed using the confocal microscope in a reflection mode [22,23]. Reflection images were collected using a confocal microscope equipped with a 60×, 1.4-NA oil-immersion lens (Nikon) and a quarter-wave plate. Specimens were illuminated with 488-nm light generated by an Innova Enterprise argon-ion laser (Coherent Laser Group, Santa Clara, CA) and the reflected (backscattered) light detected with a photomultiplier tube using a blue reflection filter. Image volumes ($153 \times 153 \times 35$ μm^3) were collected as 176 slices in a 512×512 pixel format. Collagen ECM constructs were loaded in uniaxial tension in 0.52-mm increments at a rate of 1

mm/min and paused to facilitate collection of image volumes. For these studies, image volumes were acquired at deformations below 7.8 mm (failure of specimens occurred at an applied deformation of approximately 12 mm).

Incremental Digital Volume Correlation (IDVC). Microlevel strains experienced by the 3D microstructure of the collagen ECM during mechanical loading were quantified in 3D using an IDVC algorithm. In general, the IDVC algorithm involves three main steps: (1) collection of consecutive 3D confocal images representing changes in cellular morphology and/or ECM microstructure of a tissue construct during incremental mechanical loading; (2) mathematical correlation of designated subvolumes within consecutive 3D images of the tissue construct to determine a discrete displacement field; and (3) calculation of 3D strain fields from the displacement vector fields.

A series of 3D image volumes representing changes in ECM microstructure during the application of increasing load was collected using confocal microscopy. Each image volume provided unique 3D voxel intensity patterns that allowed correlation pattern matching within consecutive images. Within each image, subvolumes were established. Each subvolume represented a group of voxels centered about a given point at which a displacement value was sought. Digital volume correlation was then used to identify the subvolume within the second image that best matched a specified subvolume within the first. Deformations were then determined between each successive set of images. Essentially, the IDVC algorithm consisted of many digital volume correlation steps to determine incremental changes in deformation and strain. These incremental deformations/strains could then be combined to determine the total deformation/strain.

The problem of digitally correlating subvolume pairs was expressed mathematically as the maximization of the cross-correlation between two 3D arrays of voxel intensity values ($\mathbf{A}$ and $\mathbf{B}$) representing the 3D collagen ECM before and after the application of an incremental load. For each trial displacement v_i, a correlation coefficient $\mathbf{R}(v_i)$ was calculated by summing the products of the intensities at all coincident image voxel locations, a_i in array $\mathbf{A}$ and $a_i + v_i$ in array $\mathbf{B}$ [Eq. (1)]. This resulted in a matrix of correlation coefficients, $\mathbf{R}$. To avoid correlating mean intensities, the average intensity (noted as $\overline{\mathbf{A}}$ and $\overline{\mathbf{B}}$) was subtracted from each image volume before correlation [Eq. (2)]. The v_i that maximized $\mathbf{R}$ defined the displacement u_i. Thus,

$$\mathbf{R}(v_i) = \sum_{x_i} \widetilde{\mathbf{A}}(x_i)\widetilde{\mathbf{B}}(x_i + v_i) \tag{1}$$

where

$$\widetilde{\mathbf{A}} = \mathbf{A} - \overline{\mathbf{A}}$$
$$\widetilde{\mathbf{B}} = \mathbf{B} - \overline{\mathbf{B}} \tag{2}$$

To improve computational efficiency, cross correlations were performed in the frequency domain where cross correlation is defined as multiplication of one function by the complex conjugate of the second. Therefore, the matrix of correlation coefficients was determined by taking the Fourier transforms of the image subvolumes, multiplying the first by the complex conjugate of the second, and then taking the inverse Fourier transform of their product

$$\mathbf{R} = \mathfrak{I}^{-1}[\mathfrak{I}(\widetilde{\mathbf{A}})\mathfrak{I}(\widetilde{\mathbf{B}})*] \tag{3}$$

Implementation of the Fourier transform to analyze the discrete data using fast Fourier transforms reduces the computation from $\vartheta[\mathrm{N}^6]$ operations [based on Eq. (1)] to $\vartheta[\mathrm{N}^3 \log_2 \mathrm{N}]$ operations [based on Eq. (3)] for the 3D cross correlation [37]. Determining the displacement that maximized $\mathbf{R}$ resulted in a measurement resolved only to the nearest voxel. Determination of strains requires displacement measurements to be resolved to a subvoxel

level. Therefore, a Gaussian peak-fitting function was implemented to interpolate the nearby values of $\mathbf{R}$ and thus obtain a more accurate measure of u_i [37].

For each u_i measured, a signal-to-noise ratio (SNR) was also determined. The SNR was defined as the maximum value of correlation coefficient matrix $\mathbf{R}(u_i)$ divided by the second highest value $\mathbf{R}(u_i')$

$$\mathrm{SNR} = \frac{\mathbf{R}(u_i)}{\mathbf{R}(u_i')} \tag{4}$$

In some cases, displacement values calculated from poorly correlated subvolumes or low SNR were filtered from the vector field. Filtered data were replaced by values linearly interpolated from nearby displacement measurements.

Incremental Procedure. For each load increment, multiple iterations were made through the correlation procedure, where the results of the previous iteration were used as a predictor for the next load increment. With a converged field of displacements for each load increment, the incremental displacements were reassembled to determine the total displacements and thus the location of each gridpoint in each load increment. Generally, the location of the point at grid location m, n, p in image t ($x_i^t|_{m,n,p}$) can be written as the sum of its initial location ($x_i^o|_{m,n,p}$) and the sum of the displacements ($u_i^s|_{m,n,p}$) from all previous increments

$$x_i^t|_{m,n,p} = x_i^o|_{m,n,p} + \sum_{s=1}^{t} u_i^s|_{m,n,p} \tag{5}$$

Since each increment determines displacements on a uniform grid, measurements for $u_i^s|_{m,n,p}$ were linearly interpolated from nearby discrete values. Applying this incremental procedure, rather than tracking the same point through all the images, made the process easily solved in parallel on several computers.

Subvolume Size and Grid Spacing. Subvolume size defined the size of the image subvolumes correlated, and further defined the domain where the algorithm searched for a displacement value. For example, correlation of two $64 \times 64 \times 32$ voxel subvolumes allowed a maximum displacement of $|u| = \{32,32,16\}$ voxels to be reliably measured. Computational time was also considered in choosing subvolume size, since doubling each dimension of the subvolume increased the computation time by eight-fold or more depending on the amount of system memory. For initial iterations, large subvolumes provide a large domain in which to converge a solution. Since later iterations have the benefit of an initial guess, small search areas can be used to substantially speed the solution.

Grid spacing defined the distances between the locations where displacements (and subsequently strains) were to be measured. For example a grid spacing of $64 \times 64 \times 32$ voxels provided a grid of $8 \times 8 \times 5$ (320) points where displacements were determined. Computational time was also a concern in selecting the grid spacing, as reducing the grid spacing in each direction by half increased the number of grid points and thus the computation time by a factor of eight.

Strain Determination. Digital image correlation resulted in a 3D array of displacement values ($u_i|_{m,n,p}$) at evenly spaced locations ($x_i|_{m,n,p}$), where (m,n,p) represents a discrete grid point. To calculate strain fields, the gradients of the displacement field (du_i/dx_j) were first determined. Numerical differentiation of the displacement field data was used to calculate these derivatives. Displacement fields were smoothed prior to numerical differentiation. For all points of the grid, except those points on the sides of the grid, centered difference finite difference equations were used to approximate the displacement gradients [38]. For points of the sides of the grid, forward and backward finite difference equations were used to calculate displacement gradients. Based upon the resulting displacement gradients, the full definition of the La-

grangian strain tensor (including linear and nonlinear portions) was then applied to calculate the strain state (ε_{ij}) at all grid locations:

$$\varepsilon_{ij} = \frac{1}{2}\left[\frac{du_i}{dx_j^o} + \frac{du_j}{dx_i^o} + \frac{du_m}{dx_i^o}\frac{du_m}{dx_j^o}\right] \qquad (6)$$

Last, the principal strains (E_k) and their associated directions (ϕ_j^k) at each spatial location were determined by solving the eigenvalue problem

$$\varepsilon_{ij}\phi_j^k = E^k\phi_j^k \qquad (7)$$

Numerical Implementation. The aforementioned techniques were integrated into a suite of MATLAB (The Mathworks, Natick, MA) functions to solve for the displacement field and eventually the strain fields from a set of confocal image volumes. Correlation of two $512\times512\times176$ image volumes (40 Mb each) through one iteration required approximately 1 h, on a personal computer with dual 866-MHz Pentium™ III microprocessors and 1.0 Gb of RAM.

Validation of Measurement Precision and Accuracy. Two methods were used to characterize measurement precision and accuracy based upon the IDVC approach: (1) correlation of multiple unloaded ($\varepsilon=0$) image data sets of a 3D tissue construct and (2) application of simulated (known) deformations to an image volume and comparison with deformation results obtained from the program.

The first method used to validate the IDVC procedure involved a comparison of two image volumes collected successively from the same 3D ECM construct to which no external mechanical load was applied. This approach represented a known ''zero-strain'' input. Confocal reflection microscopy was used to collect three pairs of image volumes representing distinct locations within a 3D collagen ECM (1 mg/ml, pH 7.4). Digital volume correlation was then used to measure the displacement fields describing the deformation of the second image volume of each pair with respect to the first. Subvolume size and grid spacing used for the digital volume correlation was altered to determine the effect of these parameters on the measurement precision and accuracy. To study the effect of subvolume size, each pair of image volumes was correlated using three different subvolume sizes: large, medium, and small. Specifically, large subvolumes were comprised of 64 $\times64\times32$ voxels and were $\approx20\times20\times10$ μm^3 in size. Similarly, medium subvolumes were comprised of $32\times32\times32$ voxels and were $\approx10\times10\times10$ μm^3 in size. Finally, small subvolumes were comprised of $16\times16\times16$ voxels and were $\approx5\times5\times5$ μm^3 in size. Since the subvolume size limits the magnitude of the displacement measurement, the first iteration through the correlation algorithm always used large subvolumes as a predictor step. Use of medium and small subvolume sizes only occurred in later iterations. Additionally, the effects of grid spacing were investigated by using three different grids: sparse, normal, and dense. The sparse grid had points spaced $64\times64\times32$ voxels ($\approx20\times20\times10$ μm^3), which resulted in a grid with $8\times8\times5$ points (320 points total). Similarly, the normal grid had points spaced $32\times32\times32$ voxels ($\approx10\times10\times10$ μm^3), which resulted in a grid with 15 $\times15\times5$ points (1125 points total). Finally, the dense grid had points spaced $16\times16\times16$ voxels ($\approx5\times5\times5$ μm^3), which resulted in a grid with $29\times29\times9$ points (7569 points total).

A second method used to verify the accuracy and precision of the algorithm involved the computational simulation of a known tensile deformation to an image volume. To simulate tensile deformation, an image volume of a 3D collagen ECM (1 mg/ml, pH 7.4) was computationally deformed in one dimension along the specimen length (1-direction) by applying a uniform displacement gradient ($du_1/dx_1^o=0.32$) in 16 increments. This was accomplished by remapping the voxel intensity patterns to new locations representing a perfectly homogeneous 1D deformation. Since the

response of a collagen ECM to a tensile load is known to be a multi-dimensional event, where deformation applied along the specimen length results in large contractions along the specimen width and thickness [24,25], the 3D deformation of a collagen ECM was also computationally simulated. The same tensile deformation was applied in the 1-direction, while contractions that were twice the magnitude of the extension were imparted in the 2-(width) and 3- (thickness) directions. For example, when a positive displacement gradient (du_1/dx_1^o) of 0.02 was applied, the corresponding transverse displacement gradients (du_2/dx_2^o and du_3/dx_3^o) were -0.04 for the first increment. Digital volume correlation was then used to measure the displacement fields describing the deformation. Subvolume size and displacement gradient increment size used for the digital volume correlation were altered to determine the effect of these parameters on the measurement precision and accuracy.

Results and Discussion

Confocal microscopy used in a reflection mode on 3D collagen ECMs generated image volumes with voxel intensity patterns that were representative of the microstructural architecture of component collagen fibrils and formed the basis of correlation pattern matching. The IDVC algorithm provided an effective means to quantify the 3D deformations and strains in the microstructure of a collagen ECM which is comprised of many fibrils.

Characterization of IDVC Measurement Precision and Accuracy. Two different techniques were used to verify algorithm operation and to identify operational constraints of the algorithm. First, measurements of displacement and strain determined from repeat unloaded image volumes of a collagen ECM verified that the algorithm accurately and precisely measured a zero- (small-) strain input. Second, measurements were taken from collagen ECM image volumes to which known simulated deformations were applied. Mean and standard deviation values for displacements (u_i), strains (ε_{ij}), and principal strains (E_i) were used to quantify measurement accuracy and precision, respectively. Ideally, true validation of the algorithm would involve a direct comparison of local 3D strain measurements within real, mechanically loaded ECM specimens as determined by IDVC with those provided by a second, independent method. However, to the best of our knowledge, no other means to estimate or measure local 3D strains are available, making such validation strategy impossible to conduct.

To remove any data resulting from poor subvolume correlation (e.g., outlier data), correlation values were initially filtered based upon a defined SNR (Refer to ''Materials and Methods'' section). Here, the filter level was established by selectively removing a percentage of data with the lowest SNR. The appropriate level of filtering to apply for data analyses was established by evaluating the standard deviation of displacement values obtained for repeat image sets of unloaded specimens as a function of filter level (Fig. 1). Specifically, displacement standard deviation was calculated as the average of standard deviation values obtained in the 1-, 2-, and 3-directions for three experimental repetitions. The effect of filtering on displacement data was also evaluated for three different subvolume sizes. Results showed that for analyses involving large subvolumes ($64\times64\times32$ voxels), displacement standard deviation or precision was consistent over the range of filtering levels evaluated. Therefore, in this case filtering was not necessary to improve precision. For smaller subvolume sizes ($32\times32\times32$ voxels and $16\times16\times16$ voxels), selective removal of data with the lowest 2% of SNRs resulted in the greatest improvement of precision. Application of filter levels greater than 2% affected only analyses performed with the smallest subvolume size ($16\times16\times16$ voxels).
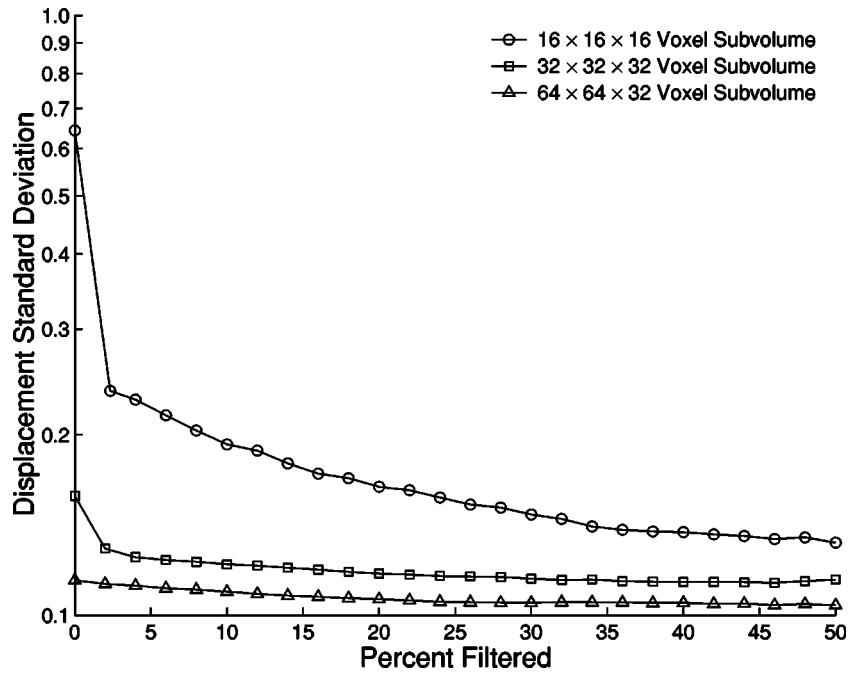
Fig. 1 The effect of filtering on displacement measurement precision (standard deviation) as a function of subvolume size. Correlation values obtained for individual subvolumes were selectively removed based upon defined signal to noise ratio.

Here, a gradual but steady decrease in displacement standard deviation was observed as the filter level was increased. Based upon these results, all subsequent data analyses were conducted with a filter level of 10%, resulting in selective elimination of correlation data with the lowest 10% SNRs.

Repeat-Unloaded Image Correlation. Displacement and strain measurements determined from three repeat image sets of unloaded collagen ECMs were averaged and the results summarized in Table 1. Measurement precision and accuracy were investigated in all three directions [1- (x-) direction, 2- (y-) direction,

Table 1 IVDC results for repeat unloaded image correlation

(a) Variation of subvolume size (normal grid)			
Subvolume	Large (64×64×32)	Medium (32×32×32)	Small (16×16×16)
u_1 (voxels)	±0.0929	±0.0925	±0.1877
u_2 (voxels)	±0.0397	±0.0523	±0.1651
u_3 (voxels)	±0.1775	±0.1944	±0.2721
ε_{11}	0.000032±0.000486	0.000012±0.000693	0.000013±0.003491
ε_{22}	−0.000058±0.000633	0.000021±0.000977	0.000174±0.003584
ε_{12}	−0.000001±0.000347	0.000003±0.000578	−0.000066±0.002641
ε_{13}	−0.000898±0.001212	−0.000909±0.001440	−0.000892±0.003056
ε_{23}	0.000116±0.001099	0.000130±0.001417	0.000044±0.003301
ε_{33}	−0.000179±0.003071	0.000098±0.003622	−0.000983±0.005950
E_1	0.002609±0.001868	0.003156±0.002381	0.005277±0.005096
E_2	0.000001±0.000500	0.000028±0.000718	−0.000031±0.002050
E_3	−0.002814±0.001785	−0.003062±0.002026	−0.006039±0.005371
(b) Variation of grid spacing (medium subvolumes)			
Grid	Sparse (8×8×5)	Normal (15×15×5)	Dense (29×29×9)
u_1 (voxels)	±0.0887	±0.0925	±0.0952
u_2 (voxels)	±0.0521	±0.0523	±0.0599
u_3 (voxels)	±0.1823	±0.1944	±0.2098
ε_{11}	0.000039±0.000405	0.000012±0.000693	0.000056±0.001454
ε_{22}	−0.000048±0.000540	0.000021±0.000977	−0.000002±0.001817
ε_{12}	−0.000003±0.000351	0.000003±0.000578	−0.000017±0.001151
ε_{13}	−0.000875±0.001048	−0.000909±0.001440	−0.000759±0.002678
ε_{23}	0.000067±0.000896	0.000130±0.001417	0.000124±0.002622
ε_{33}	−0.000162±0.003376	0.000098±0.003622	0.000614±0.006693
E_1	0.002538±0.001963	0.003156±0.002381	0.005339±0.004583
E_2	−0.000023±0.000446	0.000028±0.000718	0.000073±0.001441
E_3	−0.002763±0.002096	−0.003062±0.002026	−0.004744±0.003570

Table 2 IVDC results for one-dimensional simulated deformation

	Large subvolume ($64\times64\times32$ voxels) $du_1/dx_1\vert_{inc}=0.02$			$du_1/dx_1\vert_{inc}=0.04$		$du_1/dx_1\vert_{inc}=0.08$	
	Applied	mean$\pm$std	% error	mean$\pm$std	% error	mean$\pm$std	% error
E_1	0.3707	0.3642 ± 0.0091	1.75	0.3602 ± 0.0110	2.83	0.3512 ± 0.0165	5.26
E_2	0.0000	0.0012 ± 0.0010		0.0010 ± 0.0007		0.0009 ± 0.0008	
E_3	0.0000	-0.0015 ± 0.0012		-0.0009 ± 0.0008		-0.0011 ± 0.0007	

	Medium subvolume ($32\times32\times32$ voxels) $du_1/dx_1\vert_{inc}=0.02$			$du_1/dx_1\vert_{inc}=0.04$		$du_1/dx_1\vert_{inc}=0.08$	
	Applied	mean$\pm$std	% error	mean$\pm$std	% error	mean$\pm$std	% error
E_1	0.3707	0.3707 ± 0.0040	0.00	0.3711 ± 0.0037	0.11	0.3706 ± 0.0041	0.03
E_2	0.0000	0.0016 ± 0.0014		0.0008 ± 0.0007		0.0007 ± 0.0007	
E_3	0.0000	-0.0017 ± 0.0014		-0.0007 ± 0.0007		-0.0007 ± 0.0006	

	Small subvolume ($16\times16\times16$ voxel) $du_1/dx_1\vert_{inc}=0.02$			$du_1/dx_1\vert_{inc}=0.04$		$du_1/dx_1\vert_{inc}=0.08$	
	Applied	mean$\pm$std	% error	mean$\pm$std	% error	mean$\pm$std	% error
E_1	0.3707	0.3702 ± 0.0031	0.13	0.3705 ± 0.0019	0.05	0.3706 ± 0.0027	0.03
E_2	0.0000	0.0023 ± 0.0025		0.0010 ± 0.0008		0.0013 ± 0.0028	
E_3	0.0000	-0.0030 ± 0.0023		-0.0010 ± 0.0010		-0.0008 ± 0.0012	

and 3- (z-) direction] as subvolume size and grid spacing were varied. Mean displacement measurements are not shown since collection of repeat image volumes did not guarantee a zero displacement, mostly owing to the inability of the focus motor to reliably identify the same focal position.

In general, calculated mean strain values for all subvolume sizes and grid spacings applied were zero, demonstrating the ability of the algorithm to accurately determine a zero applied input strain. Alternatively, the standard deviation of displacement and strain measurements was used as an indicator of algorithm precision. For a given subvolume size, displacement precision was always lowest in the 3-direction, with values that were 1.5 and 4.5 times lower than those in the 1- and 2-directions. Likely, the poor precision in the 3-direction was associated with a specific z-direction aberration that results from the collection of confocal image volumes. It has been well documented that the confocal microscope has lower resolution in the 3-direction [39].

The subvolume size used to correlate the images was found to have a significant effect on displacement standard deviation or precision. Similar levels of precision were obtained for displacement measurements in all three directions with the application of large ($64\times64\times32$ voxels) and medium ($32\times32\times32$ voxels) subvolume sizes. Comparison of these results with those obtained for small ($16\times16\times16$ voxels) subvolume sizes showed a decrease in displacement precision for the small subvolume size. In the same way, a decline in the precision of strain and principal strain measurements was observed with decreasing subvolume size. This general decrease in precision as a function of subvolume size was expected, since decreasing subvolume size reduces the amount of image data (voxels) involved in each correlation analysis. For this study, each image slice was collected in a 512×512 pixel format. It is anticipated that increased sampling in the collection of images by utilizing a 1024×1024 pixel format would improve the accuracy and precision of algorithm measurements by a factor of 2.

Systematic variation of grid spacing assigned to correlated images did not significantly affect displacement precision. However, the standard deviation for strain measurements was found to be inversely proportional to grid spacing; i.e., when grid spacing was increased, strain measurements were more precise. It is evident that since strains are a function of displacement gradients (du_i/dx_j^o), any error in the displacement measurements (du_i) is amplified in the calculation of strain by the decreased spatial distance between grid points (dx_j^o).

In the present study, the 3D IDVC algorithm showed precision levels in the in-plane directions (1- and 2-direction) that were of similar magnitudes to those obtained with 2D digital image correlation (DIC). However, IDVC precision was an order of magnitude less than 2D DIC in the out-of-plane direction (3-direction). Previously, it has been reported that traditional 2D DIC methods yield precision values that are typically in the range of 0.02 pixels for displacement and 200 $\mu\varepsilon$ for strain [26]. Similar levels of precision were achieved with the 3D digital volume correlation algorithm developed by Bay and coworkers [35]. The differences in algorithm performance can likely be attributed to the increased levels of noise and ''z-direction aberration'' associated with the collection of 3D confocal images.

In summary, for measurement of small (zero) strains from repeat-unloaded images, the IDVC algorithm can be optimized through application of large subvolume sizes in association with sparse grid spacing. However, in specific cases, such as strain measurements on a cell surface or strains experienced by ECM fibrils or fibril bundles, the application of a spatially dense grid may prove beneficial since it provides increased resolution of strain measurements. Care should be taken when a spatially dense grid is used to determine such strain measurements, since the construct being studied may not satisfy continuity at the level of the measurement sought.

Simulated Deformations. To further explore IDVC as a method for determining 3D displacements and strains, both 1D and 3D deformations of a collagen ECM were simulated. One-dimensional simulations involved computationally stretching an image volume in the 1-direction to a total strain of 0.3707 at displacement gradient increments ($du_1/dx_1\vert_{inc}$) of 0.02, 0.04, 0.08, and 0.16. These simulations involved no deformation in the 2- and 3-directions. Deformations simulated in 3D involved computationally stretching the image volumes in all three directions. Here, an overall strain of 0.3707 was applied in the 1-direction while strains of -0.4339 and -0.4354 were applied in the 2- and 3-directions, respectively. For 3D deformations, the incremental displacement gradients applied in the 2- and 3-directions were twice the step value used in the 1-direction so as to reflect the 3D deformation observed experimentally for collagen ECMs [24,25]. It should be noted that as the incremental displacement gradient increased, fewer image volumes were involved in the overall correlation analysis. The effect of subvolume size was also determined as part of these analyses.

Principal strains (means$\pm$standard deviation of all subvolumes) measured for 1D deformation simulations as a function of applied displacement gradient increment and subvolume size are summarized in Table 2. Algorithm results did not converge for any of the

Table 3 IVDC results for three-dimensional simulated deformation

		Large subvolume (64×64×32 voxel) $du_1/dx_1|_{inc}=0.02$	
	Applied	mean±std	% error
E_1	0.3707	0.3623±0.0233	2.27
E_2	−0.4339	−0.4315±0.0047	0.55
E_3	−0.4354	−0.4455±0.0043	2.32
		Medium subvolume (32×32×32 voxel) $du_1/dx_1|_{inc}=0.02$	
	Applied	mean±std	% error
E_1	0.3707	0.3793±0.0129	2.32
E_2	−0.4339	−0.4345±0.0021	0.14
E_3	−0.4354	−0.4422±0.0036	1.56

subvolume sizes evaluated when the large (0.16) displacement gradient increment was applied. For an applied displacement gradient increment of 0.02, the maximum principal strain (E_1) strain was measured as 0.3642, 0.3707, and 0.3702 for large, medium, and small subvolumes, respectively. These results accurately reflected the applied value of 0.3707 with a percent error ranging from 0 to 1.75%. All other principal strain components measured for this specific displacement gradient were close to zero, with a maximum absolute error of 0.0030. Despite the incremental displacement gradient applied, the accuracy of E_1 measurements improved significantly for analyses involving medium and small subvolumes. When the displacement gradient was increased, a decrease in E_1 accuracy and precision was noted, but only for analyses involving large subvolumes. Changes in displacement gradient yielded E_1 measurements of comparable accuracy and precision when medium and small subvolumes were used. Evaluation of E_2 and E_3 results showed that similar levels of accuracy and precision were obtained despite the displacement gradient increment and subvolume size used in the analysis.

Algorithm performance for simulated deformations in 3D was also evaluated as a function of subvolume size and displacement gradient increment (Table 3). Interestingly, algorithm results converged only when a displacement gradient of 0.02 was applied. The algorithm did not converge for analyses involving small subvolume sizes. Comparison of results revealed that use of medium subvolume size provided the best levels of precision and accuracy for principal strain measurements for these simulated deformation experiments. Together, Tables 2 and 3 shows that, in general, a reduction in subvolume size improved the accuracy and precision of strain calculations. For 3D simulated deformations, the second and third principal strains were much more precise even though the applied strains were larger. A potential explanation for this observation is that as the volume was computationally deformed, component collagen fibrils tended to align in the direction of the simulated stretch. This alignment likely caused a loss of intensity gradients (variations in voxel intensity values that comprise the 3D images) along the 1-direction, but preserved intensity gradients in the transverse directions. The use of small subvolumes sizes to improve accuracy and precision of strain measurements for large strain analyses is in direct contrast to those results obtained for zero- or small- strain input experiments. When images volumes of structures that experience large relative deformations are compared, image data near the periphery of subvolumes used for correlation pattern matching undergo a much larger relative deformation than image data near the center of the subvolumes. As such, application of a large subvolume size may introduce increased noise into the correlation procedures involving large strain analyses, thus reducing both accuracy and precision.

In addition, displacement gradient increment requirements for 3D simulated deformations were found to be more restrictive than those for 1D simulations. Such results can be explained by comparing the Von Mises equivalent strains (ε_{eq}) for both simulations as calculated below

$$\varepsilon_{eq}=\sqrt{\varepsilon_{11}^2+\varepsilon_{22}^2+\varepsilon_{33}^2} \qquad (8)$$

For the 1D simulated stretch, acceptable measures of the strain state were obtained for displacement gradients of 0.08 and below, which corresponds to a Von Mises equivalent strain of 0.08 or less. However, simulated deformations in 3D required incremental displacement gradients of 0.02, 0.04, and 0.04 in the 1-, 2-, and 3- directions, respectively. These values of applied strain correspond to a ε_{eq} of 0.06. Therefore, it is apparent that the algorithm functioned reasonably well as long as the ε_{eq} applied at each strain increment was less than approximately 0.10. Therefore, for analysis of experimental data involving mechanically loaded collagen ECMs (in which a 1D stretch causes 3D deformation), incremental deformations should not exceed a ε_{eq} of 0.10.

In summary, these results indicate that the IDVC algorithm effectively predicts the known 3D strain state of a collagen ECM at the local level. Algorithm parameters such as subvolume size and incremental displacement gradient can be adjusted to yield strain measurements with error rates of 2.5% or less. Based on these test data, when applied to a series of images with a similar level of deformation between images, IDVC should result in similar accuracy and precision as demonstrated here.

Measurement of the Local 3D Strain State of a Collagen ECM Under Tensile Load. Application of IDVC to a series of image volumes representing a collagen ECM loaded incrementally in tension allowed determination of the local 3D strain history of collagen ECM microstructure. Visualization of the 3D time-varying response of a collagen ECM microstructure to uniaxial tensile strain using confocal microscopy in a reflection mode has been demonstrated previously [25]. IDVC provided a method by which deformations experienced by collagen fibrils observed qualitatively could be translated to quantifiable micro- (local) level displacements and strains in 3D. IDVC was applied to a series of image volumes representing a collagen ECM (polymerized at 1 mg/ml collagen concentration and pH 7.4) subjected to a uniaxial tensile load of 7.8 mm. This subfailure load, which corresponded to a strain of approximately 0.35, was chosen based upon the stress-strain properties for such matrices as determined previously by our laboratory [24]. The load was applied in steps of 0.52 mm so to provide an incremental displacement gradient of 0.02. Based upon data generated from the simulated deformation experiments, application of displacement gradient increments less than 0.02 would provide improved levels of accuracy and precision; however, such step sizes led to practical difficulties (e.g., total time required to complete an experiment) in evaluating the local mechanical behavior of collagen ECMs at large strain levels.

The ability of the IDVC algorithm to effectively track a given image subvolume surrounding a single grid point (necessary step to make deformation measurements and determine strains) was established upon visual inspection of the sequential confocal images. Figure 2 shows the progressive deformation of component collagen fibrils at each load increment. Although the first and last images were not recognizably similar, each pair of successive images had similar voxel intensity patterns, which provided the basis of the correlation analysis. Movies showing the progressive deformation of a collagen ECM microstructure in response to increased tensile loading can be viewed at http://www.cyto.purdue.edu/IVDC/videos.htm (Video 1).

Based upon these qualitative data, quantification of the local 3D strain response was initiated by the assignment of grid points to the undeformed image in order to establish appropriately sized image subvolumes [Fig. 3(a)]. It should be noted that the volume of points correlated ($\approx 100\times100\times25$ μm^3) represented 32% of the imaged volume ($\approx 150\times150\times35$ μm^3) and a much smaller percentage (0.000025%) of the overall specimen volume. The load-dependent deformation of the initial image could be readily
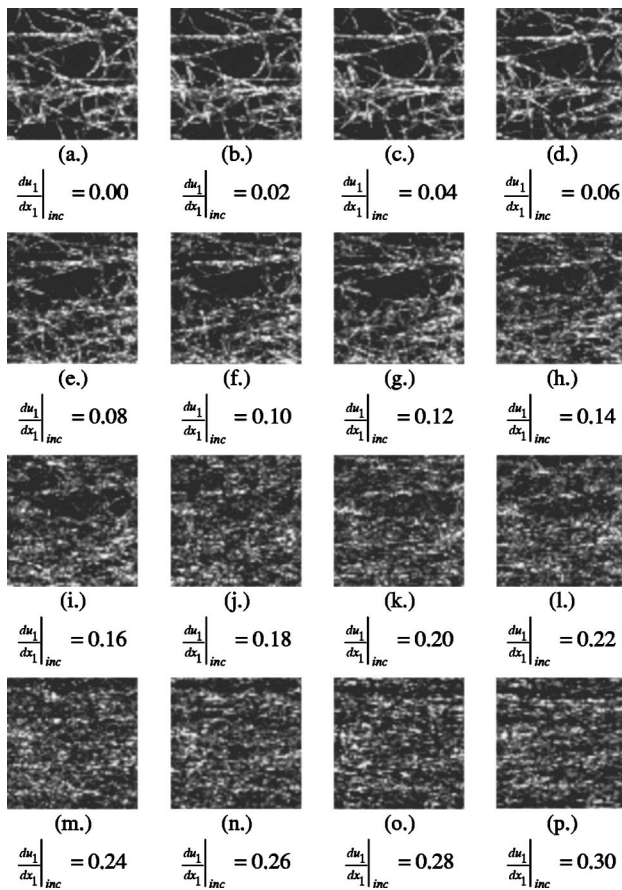
Fig. 2 A series of 3D confocal reflection images (shown as 2D projections) representing a correlated subvolume within a collagen ECM during incremental mechanical loading as tracked by the IVDC algorithm

appreciated by plotting the incremental changes in grid point positions [Figs. 3(b)–3(d)]. Additionally, the maximum principal strain as determined by the IDVC algorithm is plotted on the contour. A movie showing the contours of maximum principal strains throughout the imaged volume at increasing load levels can be seen at http://www.cyto.purdue.edu/IVDC/videos.htm (Video 2). Another presentation of the 3D local-level strain state
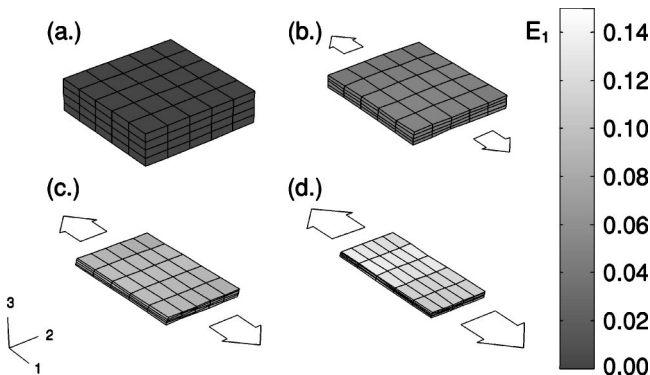
Fig. 3 Progressive volumetric deformation and changes in the microlevel strain distribution for a region within a mechanically loaded collagen ECM. Maximum principle strain (extensional stretch) is plotted on the contour for applied macro level strains of (a) 0; (b) 0.1; (c) 0.2; and (d) 0.3. Original image represents a 100×100×25 μm^3 volume within the collagen ECM.

of the mechanically loaded collagen ECM was provided by an evaluation of the six independent components of the Langrangian strain (ε_{ij}) as a function of the applied deformation (Fig. 4). All deformations and strains within the image volume appeared homogeneous in magnitude, as noted by the strain contours (Fig. 3) and the small variation (standard deviation) in principal strain measurements (Fig. 4). These results showed that while the mechanical deformation was applied in the 1-direction, the largest deformations occurred in the transverse (2- and 3-) directions and all shear strains remained near zero. A significant transverse contraction was observed in the strain through the thickness (ε_{ij}), which approached −0.50. Note that a Lagrangian strain of this magnitude corresponds to the dimension reducing to zero. Qualitatively, these results are consistent with visualizations of collagen ECMs loaded in tension, where significant transverse contractions were observed both macroscopically [24] and microscopically [25]. Quantitatively, macroscopic measurements regarding the reduction in the width and thickness dimension of the gauge section of the specimen [25] correlate well with those measured microscopically from the ECM microstructure in the present study.

Note that the length scale of the local strain measurements ($\approx$20.0 μm) in theses studies was much larger than the size of an individual collagen fibril ($\approx$0.4 μm). As such, the strains measured in this paper are strains in the microstructure of the collagen ECM, not strains in a single fibril. The IDVC algorithm assumes the collagen ECM microstructure to be a continuum. This assumption is consistent with many microstructural models of the ECM used to predict the behavior of tissues [17,40–48].

A practical requirement of our experimental setup which involves the integration of a miniature mechanical loading device with a confocal microscope is that images are acquired during pauses (approximately 5–10 min) in the mechanical loading [25]. During the imaging process the specimen was held isometrically, virtually eliminating vibrations of the sample and any unanticipated failure during collection of 3D images. Additionally, IDVC was effective at determining the 3D local strain state of collagen ECMs at subfailure tensile strain levels of nearly 0.40 and below. Resolution of the fibrous microstructure of the collagen ECM at higher strain levels or near failure strain levels is limited by the alignment and compaction of fibrils in the direction of loading (see Fig. 2). It has been shown that biaxial loading does not cause unidirectional fibrillar alignment within collagenous tissues [49]. Therefore, this IDVC algorithm could possibly perform even better for biaxial or possibly even triaxial experimental data.

In conclusion, as demonstrated on both calibration and real data obtained with confocal reflection microscopy, IDVC allowed accurate and precise quantification of 3D large deformation and strains in collagen ECM microstructures under applied mechanical load. We are currently utilizing IDVC to determine the effect of collagen microarchitecture on the 3D strain response at the microscopic level. IDVC can also be applied to tissue constructs, in which cells are cultured within 3D collagen ECMs. IDVC would provide much-needed quantitative descriptions of the micromechanical interactions between cells and their surrounding ECM and subsequent effects on tissue structure and function. For such studies, cells within the tissue construct should be stained with a vital fluorescent dye. Reflected light from the collagen fibrils can then be collected simultaneously with cell-based fluorescence using confocal microscopy in a combined reflection-epifluorescence mode [23,25]. In this way, fluorescence images representing an individual cell within the tissue construct provide intensity gradients that are suitable for digital volume correlation. Recently, such a strategy has been implemented in our lab for determining 3D microlevel strain states of both an individual cell and its surrounding ECM induced by (1) application of external mechanical loads and (2) ECM remodeling by cells over time. Precise measurements characterizing the 3D strain state of the local microenvironment of an individual cell will also make it possible to relate a particular cellular response such as changes in
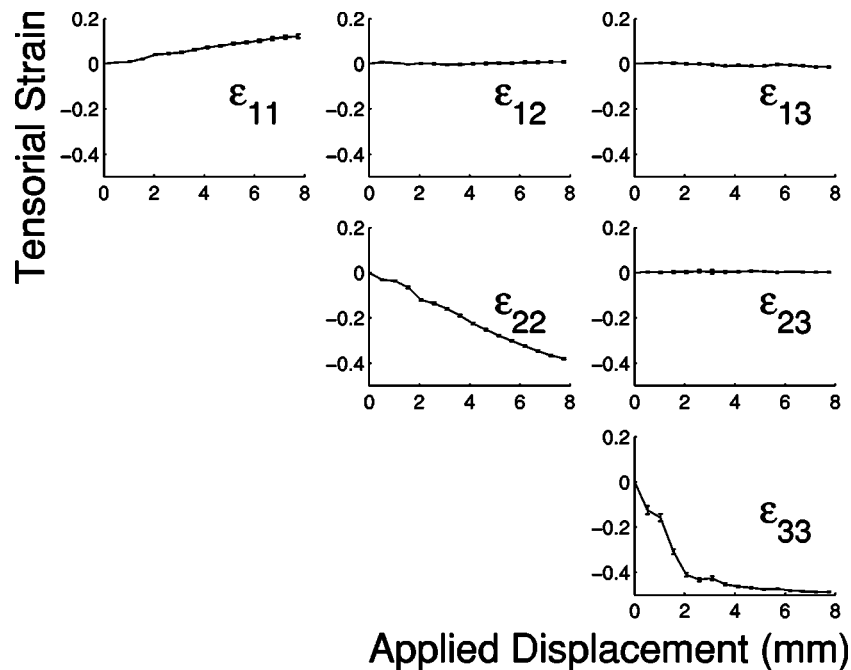
Fig. 4 Changes in the six independent components of the Lagrangian strain (means over the entire volume evaluated) as the external mechanical load was incrementally increased. Error bars indicate standard deviation.

gene expression, cytoskeleton organization, ion fluxes, morphology, and adhesion properties to a specific extracellular loading state. Such data are essential to further the development of models describing tissue construct biomechanics [40–45] as well as to advance the definition of the mechanisms involved in mechanotransduction.

Acknowledgments

References

[1] Brown, T. D., 2000, "Techniques for Mechanical Stimulation of Cells *In Vitro*: A Review," J. Biomech., **33**, pp. 3–14.
[2] Tomasek, J. J., Gabbiani, G., Hinz, B., Chaponnier, C., and Brown, R. A., 2002, "Myofibroblasts and Mechanoregulation of Connective Tissue Remodeling," Nat. Rev. Mol. Cell Biol., **3**, pp. 349–363.
[3] Roy, P., Rajfur, Z., Pomorski, P., and Jacobson, K., 2002, "Microscope-Based Techniques to Study Cell Adhesion and Migration," Nat. Cell Biol., **4**, pp. E91–E96.
[4] Harris, A. K., Wild, P., and Stopak, D., 1980, "Silicone Rubber Substrata: A New Wrinkle in the Study of Cell Locomotion," Science, **208**, pp. 177–179.
[5] Pelham, R. J., and Wang, Y.-L., 1997, "Cell Locomotion and Focal Adhesions are Regulated by Substrate Flexibility," Proc. Natl. Acad. Sci. U.S.A., **94**, pp. 13661–13665.
[6] Roy, P., Petroll, W. M., Cavanagh, H. D., Chuong, C. J., and Jester, J. V., 1997, "An *In Vitro* Force Measurement Assay to Study the Early Mechanical Interaction Between Corneal Fibroblasts and Collagen Matrix," Exp. Cell Res., **232**, pp. 106–117.
[7] Fung, Y. C., 1993, *Biomechanics: Mechanical Properties of Living Tissues*, Springer-Verlag, New York.
[8] Eastwood, M., Mudera, V. C., McGrouther, D. A., and Brown, R. A., 1998, "Effect of Precise Mechanical Loading on Fibroblasts Populated Collagen Lattices: Morphological Changes," Cell Motil. Cytoskeleton, **40**, pp. 13–21.
[9] Butt, R. O., Laurent, G. J., and Bishop, J. E., 1995, "Mechanical Load and Polypeptide Growth Factors Stimulate Cardiac Fibroblasts Activity," Ann. N.Y. Acad. Sci., **752**, pp. 387–393.
[10] Varedi, M., Tredget, E. E., Ghahary, A., and Scott, P. G., 2000, "Stress-Relaxation and Contraction of a Collagen Matrix Induces Expression of TGF-Beta and Triggers Apoptosis in Dermal Fibroblasts," Biochem. Cell Biol., **78**, pp. 427–436.
[11] He, Y., and Grinnell, F., 1994, "Stress Relaxation of Fibroblasts Activates a Cyclic AMP Signaling Pathway," J. Cell Biol., **126**, pp. 457–464.
[12] Carver, W., Nagpal, M. L., Nachtigal, M., Borg, T. K., and Terracio, L., 1991, "Collagen Expression in Mechanically Stimulated Cardiac Fibroblasts," Circ. Res., **69**, pp. 116–122.
[13] Lambert, C. A., Soudant, E. P., Nusgens, B. V., and Lapiere, C. M., 1992, "Pretranslational Regulation of Extracellular Matrix Molecules and Collagenase Expression in Fibroblasts by Mechanical Forces," Lab. Invest., **66**, pp. 444–451.
[14] Chiquet-Ehrismann, R., Tannheimer, M., Koch, M., Brunner, A., Spring, J., and Martin, D., 1994, "Tenascin C Expression by Fibroblasts is Elevated in Stressed Collagen Gels," J. Cell Biol., **127**, pp. 2093–2101.
[15] Prajapati, R. T., Chavally-Mis, B., Herbage, D., Eastwood, M., and Brown, R. A., 2000, "Mechanical Loading Regulates Protease Production by Fibroblasts in Three-Dimensional Collagen Substrates," Wound Repair Regen, **8**, pp. 226–237.
[16] Kessler, D., Dethlefsen, S. W., Haases, I., Plomann, M., Hirche, F., Krieg, T., and Eckes, B., 2001, "Fibroblasts in Mechanically Stressed Collagen Lattices Assume a "Synthetic" Phenotype," J. Biol. Chem., **276**, pp. 36575–36585.
[17] Mow, V. C., Bachrach, N. M., Setton, L. A., and Guilak, F., 1994, "Stress, Strain, Pressure and Flow Fields in Articular Cartilage and Chondrocytes," *Cell Mechanics and Cellular Engineering*, Mow, V. C., Guilak, F., Tran-Son-Tay, R., and Hochmuth, R. M. eds., Springer-Verlag, New York, pp. 345–379.
[18] Guilak, F., 1994, "Volume and Surface Area Measurement of Viable Chondrocytes in Situ Using Geometric Modeling of Serial Confocal Sections," J. Microsc. (Paris), **173**, pp. 245–256.
[19] Guilak, F., Ratcliff, A., and Mow, V. C., 1995, "Chondrocyte Deformation and Local Tissue Strain in Articular Cartilage: A Confocal Microscopy Study," J. Orthop. Res., **13**, pp. 410–442.
[20] Lee, D. A., Knight, M. M., Bolton, J. F., Idowu, B. D., Kayser, M. V., and Bader, D. L., 2000, "Chondrocyte Deformation Within Compressed Agarose Constructs at the Cellular and Subcellular Levels," J. Biomech., **33**, pp. 81–95.
[21] Knight, M. M., van de Breevaart Bravenboer, J., Lee, D. A., van Osch, G. J. V. M., Weinans, H., and Bader, D. L., 2002, "Cell and Nucleus Deformation in Compressed Chrondrocyte-Alginate Constructs: Temporal Changes and Calculation of Cell Modulus," Biochim. Biophys. Acta, **1570**, pp. 1–8.
[22] Brightman, A. O., Rajwa, B. P., Sturgis, J. E., McCallister, M. E., Robinson, J. P., and Voytik-Harbin, S. L., 2000, "Time-Lapse Confocal Reflection Microscopy of Collagen Fibrillogenesis and Extracellular Matrix Assembly *In Vitro*," Biopolymers, **54**, pp. 222–234.
[23] Voytik-Harbin, S. L., Rajwa, B. P., and Robinson, J. P., 2001, "3D Imaging of ECM and ECM-Cell Interactions," Methods Cell Biol., **63**, pp. 583–596.
[24] Roeder, B. A., Kokini, K., Sturgis, J. E., Robinson, J. P., and Voytik-Harbin, S. L., 2002, "Tensile Mechanical Properties of Three-Dimensional Type I Col-

lagen Extracellular Matrices With Varied Microstructure," J. Biomech. Eng., **124**, pp. 214–222.

[25] Voytik-Harbin, S. L., Roeder, B. A., Sturgis, J. E., Kokini, K., and Robinson, J. P., 2003, "Simultaneous Mechanical Loading and Confocal Reflection Microscopy for 3D Microbiomechanical Analysis of Biomaterials and Tissue Constructs," Microsc. Microanal., **9**(1), pp. 74–85.

[26] Chu, T. C., Ranson, W. F., Sutton, M. A., and Peters, W. H., 1985, "Applications of Digital-Image-Correlation Techniques to Experimental Mechanics," Exp. Mech., **25**, pp. 232–244.

[27] Kahn-Jetter, Z. L., Jha, N. K., and Bhatia, H., 1994, "Optimal Image Correlation in Experimental Mechanics," Opt. Eng., **33**, pp. 1099–1105.

[28] Lyons, J. S., Liu, J., and Sutton, M. A., 1996, "High-Temperature Deformation Measurements Using Digital-Image Correlation," Exp. Mech., **36**, pp. 64–70.

[29] McNeill, S. R., Peters, W. H., and Sutton, M. A., 1987, "Estimation of Stress Intensity Factor by Digital Image Correlation," Eng. Fract. Mech., **28**, pp. 101–112.

[30] Lee, J., Leonard, M., Oliver, T., Ishihara, A., and Jacobson, K., 1994, "Traction Forces Generated by Locomoting Keratocytes," J. Cell Biol., **127**, pp. 1957–1964.

[31] Dembo, M., and Wang, Y. L., 1999, "Stresses at the Cell-to-Substrate Interface During Locomotion of Fibroblasts," Biophys. J., **76**(4), pp. 2307–2316.

[32] Pelham, R. J., and Wang, Y.-L., 1999, "High Resolution Detection of Mechanical Forces Exerted by Locomoting Fibroblasts on the Substrate," Mol. Biol. Cell, **10**, pp. 935–945.

[33] Tolic-Norrelykke, I. V., Butler, J. P., Chen, J., and Wang, N., 2002, "Spatial and Temporal Traction Response in Human Airway Smooth Muscle Cells," Am. J. Phys. Cell Physiol., **283**, pp. C1254–C1266.

[34] Wang, C. C.-B., Deng, J.-M., Athesian, G. A., and Hung, C. T., 2002, "An Automated Approach for Direct Measurement of Two-Dimensional Strain Distributions Within Articular Cartilage Under Unconfined Compression," J. Biomech. Eng., **124**, pp. 557–567.

[35] Bay, B. K., Smith, T. S., Fyhrie, D. P., and Saad, M., 1999, "Digital Volume Correlation: Three-Dimensional Strain Mapping Using X-Ray Tomography," Exp. Mech., **39**, pp. 217–226.

[36] Smith, T. S., Bay, B. K., and Rashid, M. M., 2002, "Digital Volume Correlation Including Rotational Degrees of Freedom During Minimization," Exp. Mech., **42**(3), pp. 272–278.

[37] Raffel, M., Willert, C., and Kompenhans, J., 1998, *Particle Image Velocimetry: A Practical Guide*, Springer-Verlag, Berlin.

[38] Hoffman, J. D., 1992, *Numerical Methods for Engineers and Scientists*, McGraw-Hill, New York.

[39] Pawley, J. B., 1995, *Handbook of Biological Confocal Microscopy*, 2nd ed., Plenum Press, New York.

[40] Barocas, V. H., and Tranquillo, R. T., 1994, "Biphasic Theory and *In Vitro* Assays of Cell-Fibril Interaction in Tissue-Equivalent Gels," *Cell Mechanics and Cellular Engineering*, Mow, V. C., Guilak, F., Tran-Son-Tay, R., and Hockmuth, R. M., eds., Springer-Verlag, New York, pp. 185–209.

[41] Barocas, V. H., and Tranquillo, R. T., 1997, "A Finite Element Solution for the Anisotropic Biphasic Theory of Tissue-Equivalent Mechanics: The Effect of Contact Guidance on Isometric Cell Traction Measurement," J. Biomech. Eng., **119**, pp. 137–145.

[42] Barocas, V. H., and Tranquillo, R. T., 1997, "An Anisotropic Biphasic Theory of Tissue-Equivalent Mechanics: The Interplay Among Cell Traction, Fibrillar Network Deformation, Fibril Alignment and Cell Contact Guidance," J. Biomech. Eng., **119**, pp. 261–268.

[43] Agoram, B., and Barocas, V. H., 2001, "Coupled Macroscopic and Microscopic Scale Modeling of Fibrillar Tissues and Tissue Equivalents," J. Biomech. Eng., **123**, pp. 362–369.

[44] Zhalak, G. I., Wagenseil, J. E., Wakatsuki, T., and Elson, E. L., 2000, "A Cell-Based Constitutive Relation for Bio-Artificial Tissues," Biophys. J., **79**, pp. 2369–2381.

[45] Breuls, R. G. M., Sengers, B. G., Oomens, C. W. J., Bouten, C. V. C., and Baaijens, F. P. T., 2002, "Predicting Local Cell Deformation in Engineered Tissue Constructs: A Multilevel Finite Element Approach," J. Biomech. Eng., **124**, pp. 198–207.

[46] Mow, V. C., Kwan, M. K., Lai, W. M., and Holmes, M. H., 1994, "A Finite Deformation Theory for Nonlinearly Permeable Soft Hydrated Biological Tissues," *Frontiers in Biomechanics*, Schmid-Schoenbein, G. W., Woo, S. L.-Y., and Zweifach, B. W., eds., Springer-Verlag, New York, pp. 153–179.

[47] Wren, T. A. L., and Carter, D. R., 1998, "A Microstructural Model for the Tensile Constitutive Failure Behavior of Soft Skeletal Connective Tissues," J. Biomech. Eng., **120**, pp. 55–61.

[48] Guilak, F., and Mow, V. C., 2000, "The Mechanical Environment of the Chondrocytes: A Biphasic Finite Element Model of Cell-Matrix Interactions in Articular Cartilage," J. Biomech., **33**, pp. 1663–1673.

[49] Billiar, K. L., and Sacks, M. S., 1997, "A Method to Quantify the Fiber Kinematics of Planar Tissues Under Biaxial Stretch," J. Biomech., **30**, pp. 753–756.